The Partition of Unity Finite Element Method for the simulation of waves in air and poroelastic media

Jean-Daniel Chazot[a] and Emmanuel Perrey-Debain
Université de Technologie de Compiègne, Laboratoire Roberval UMR 7337, CS 60319, 60203 Compiègne cedex, France

Benoit Nennig
Laboratoire d'Ingénierie des Systèmes Mécaniques et des Matériaux (LISMMA), SUPMECA, 3 rue Fernand Hainaut, 93407 Saint-Ouen, France

(Received 20 June 2013; revised 15 November 2013; accepted 25 November 2013)

Recently Chazot *et al*. [J. Sound Vib. **332**, 1918–1929 (2013)] applied the Partition of Unity Finite Element Method for the analysis of interior sound fields with absorbing materials. The method was shown to allow a substantial reduction of the number of degrees of freedom compared to the standard Finite Element Method. The work is however restricted to a certain class of absorbing materials that react like an equivalent fluid. This paper presents an extension of the method to the numerical simulation of Biot's waves in poroelastic materials. The technique relies mainly on expanding the elastic displacement as well as the fluid phase pressure using sets of plane waves which are solutions to the governing partial differential equations. To show the interest of the method for tackling problems of practical interests, poroelastic-acoustic coupling conditions as well as fixed or sliding edge conditions are presented and numerically tested. It is shown that the technique is a good candidate for solving noise control problems at medium and high frequency.
 [http://dx.doi.org/10.1121/1.4845315]

PACS number(s): 43.55.Ka, 43.20.Gp, 43.50.Gf, 43.20.Jr [FCS] Pages: 724–733

I. INTRODUCTION

In this work, we are concerned with the numerical simulation of sound pressure field in enclosed cavities in which absorbing porous materials are present. The type of applications we have in mind ranges from room acoustics predictions, sound proofing of aircraft or cars' passenger compartments, to muffler designs in Heat, Ventilation, and Air-Conditioning systems. If the presence of absorbers can sometimes be modeled with a normal incidence impedance boundary condition, a precise description of the sound field which is valid in all cases requires the discretization of the absorbing materials as well.[1] Furthermore, for a certain class of absorbent materials such as polymer foams the solid structure has a finite stiffness. In this case, Biot's theory describing the propagation of elastic and pressure waves in the poroelastic material must be used.[2] The numerical solution of Biot's equations using the finite element method (FEM) has been extensively discussed in the literature and various formulations involving different variables have been proposed; see, for instance, Refs. 3–5, as well as quoted references in Ref. 6. In this regard, the mixed $(\boldsymbol{u}, p_p)$ formulation of Atalla *et al*. offers the great computational advantage of reducing the number of degrees of freedom as well as easing the transmission conditions at the air-porous interface.[4] Despite the progress being made, the classical finite element discretization of the mixed formulation is known to suffer from slow convergence rates, i.e., with respect to the number of degrees of freedom required to achieve reliable results.[6,7] The reasons for this lie in the biphasic nature of the poroelastic medium and the disparity of scales between wavenumbers associated with the different type of waves allowed to propagate in the material. This is discussed in Ref. 8 and shown in Ref. 9 using the displacement formulation. These limitations restrict the finite element analysis of poroelastic materials to reduced-sized configurations. To alleviate this convergence problem, the development of high-order hierarchical elements was considered in Refs. 8, 10, and 11. Modal reduction techniques were also investigated in Refs. 12–16. Alternatively, boundary integral formulations and their discretized versions, the boundary element method, can be used via the explicit knowledge of the Green's tensor of the poroelastic wave equations.[17] In another domain, the Padé approximant method has also been used efficiently with shell elements in Ref. 18 to model multilayered structures with poroelastic materials.

All the approaches cited above have in common that the unknown oscillatory solutions (pressure or displacement fields) are approximated using piecewise polynomial shape functions. The last decade has seen the emergence of new approaches in which the solution to the problem is expanded in the basis of wave functions, usually taking the form of plane, cylindrical, or spherical waves. In essence, these functions capture the oscillatory character of the wave field thus allowing to tackle medium to high frequency problems.[19] The idea was first developed to the Helmholtz equation giving rise to, to name but a few, the Partition of Unity Finite Element Method (PUFEM),[20,21] the Ultra-Weak formulation,[22,23] the Discontinuous Galerkin Method,[24,25] the Wave

[a]Author to whom correspondence should be addressed. Electronic mail: jean-daniel. chazot@utc.fr

 0001-4966/2014/135(2)/724/10/$30.00

Boundary Element Method,[26] the Wave Based Method,[27,28] the Variational Theory of Complex Rays,[29] and, to some extent, the Method of Fundamental Solutions.[30] Extension to the elastic wave equation can be found in Refs. 31 and 32, for instance. Applications to Biot's poroelastic wave equations have received little attention so far; we can cite three recent research works in this direction in Refs. 33–35. All these methods offer a drastic reduction in degrees of freedom as compared with conventional discretization schemes. Among these techniques, the PUFEM has the advantage to be very similar to the FEM and its numerical implementation can be easily adapted to any FEM mesh.

In a recent paper,[36] the present authors applied the PUFEM for the analysis of interior sound fields with absorbing materials. The work is, however, restricted to a certain class of absorbing materials that react like an equivalent fluid. This paper presents an extension of the method to the numerical simulation of Biot's waves in poroelastic materials in the two-dimensional case. The paper is organized as follows. The PUFEM formulation is presented in Sec. II. In the porous domain, the pressure and displacement fields are discretized using sets of plane waves with complex wavenumbers and the classical coupling conditions at the air-porous interface are enforced by the use of Lagrange multipliers. In Sec. III, the performances of the method, measured in terms of data reduction, are assessed for an artificial problem for which analytical solutions are available. In Sec. IV, the interest of the method is illustrated on various examples of practical interest such as the analysis of interior sound fields in a car's passenger compartment.

II. FORMULATION

A. Problem statement and governing equations

The general interior problem under consideration is illustrated in Fig. 1. It consists of a bounded two-dimensional domain $V = V_a \cup V_p$ where V_a is an air-filled cavity with density ρ_a and sound speed c_a and the domain V_p is filled with a poroelastic material. For a brief nomenclature, all quantities associated with the air cavity are referred by the subscript a, whereas the porous domain is denoted by the subscript p. We call S_c the air-porous interface and S_a and S_p the remaining part of the boundary of each domain. In the frequency domain (the time dependence $e^{-i\omega t}$ is assumed),

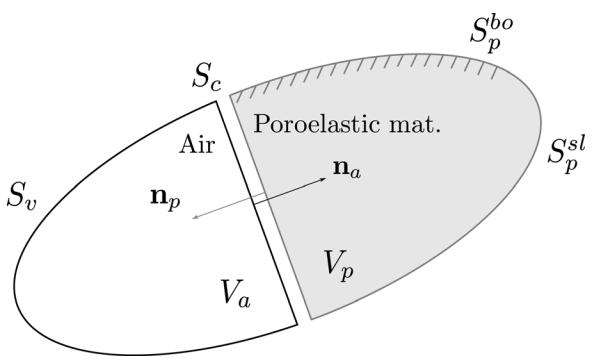

FIG. 1. Studied case and notations.

the governing equation for the acoustic pressure in the air is the classical Helmholtz equation

$$\Delta p_a + k_a^2 p_a = 0, \tag{1}$$

where $k_a = \omega/c_a$ is the wavenumber and ω is the angular frequency. The wave propagation involving, respectively, the fluid and solid phases displacement $\boldsymbol{U}$ and $\boldsymbol{u}$ in the poroelastic medium is described by the Biot-Allard model which is well documented in the reference textbook.[2] These equations can be written in a reduced form using only the solid displacement and the fluid pressure p_p as

$$\nabla \cdot \boldsymbol{\sigma}^s + \omega^2 \rho \boldsymbol{u} = -\gamma \nabla p_p, \tag{2}$$

$$\Delta p_p + \omega^2 \frac{\rho_{22}}{R} p_p = \omega^2 \gamma \frac{\rho_{22}}{\phi^2} \nabla \cdot \boldsymbol{u}. \tag{3}$$

Here, ϕ is the porosity of the porous material, $\gamma = \phi(\rho_{12}/\rho_{22} - Q/R)$ and $\rho = \rho_{11} - \rho_{12}^2/\rho_{22}$. The effective density coefficient, ρ_{11}, ρ_{22}, respectively for the solid phase and the fluid phase, and the coupling density coefficient ρ_{12}, are complex and the imaginary part takes into account the viscous damping. The *in vacuo* stress tensor $\boldsymbol{\sigma}^s$ reads

$$\boldsymbol{\sigma}^s = \mathbf{I}\left(K_b - \frac{2}{3}N\right)\nabla \cdot \boldsymbol{u} + 2N\boldsymbol{\varepsilon}, \tag{4}$$

with $\boldsymbol{\varepsilon}$ the *in vacuo* strain tensor. Here, K_b is the complex dynamic bulk modulus of the frame. The shear modulus N includes the structural damping, R is the effective bulk modulus of the fluid phase, and Q indicates the coupling of the two phase volumic dilatation. All these coefficients are related to the poroelastic structural parameters[37,38] (namely, the flow resistivity σ, the tortuosity α_∞, the viscous and thermal characteristic lengths Λ and Λ', the Poisson coefficient ν, and the effective skeleton density ρ_1) by the Johnson-Champoux-Allard model. For completeness, their value for the XFM foam which has been chosen in our applications is reminded in Table I. Coupling conditions between the acoustic domain and the poroelastic material are summarized by Debergue *et al.*:[39]

$$\boldsymbol{\sigma}\mathbf{n}_p = -p_a \mathbf{n}_p, \tag{5}$$

$$p_p = p_a, \tag{6}$$

$$\phi(U_n - u_n) + u_n = \frac{1}{\rho_a \omega^2} \frac{\partial p_a}{\partial n_p}. \tag{7}$$

The first condition is the standard continuity requirement of the normal stress at the interface [here $\sigma = \sigma^s - \phi p_p(1 + Q/R)\boldsymbol{I}$ denotes the total stress tensor]. The second condition ensures the continuity of the pressure between the

TABLE I. Material properties.

Foam	ϕ	σ (10^3Nm^{-4}s)	α_∞	Λ (μm)	Λ' (μm)	ρ_1 (kgm^{-3})	N (kPa)	ν
XFM	0.98	13.5	1.7	80	160	30	200(1 − 0.05i)	0.35

acoustic domain and the pores. The last condition ensures the continuity of the normal displacement at the interface. Note that for the sake of clarity, we put $U_n = \boldsymbol{U} \cdot \boldsymbol{n}_p$ and $u_n = \boldsymbol{u} \cdot \boldsymbol{n}_p$. On the other part of the boundary of the air cavity, a prescribed normal velocity v_a is imposed,

$$\frac{\partial p_a}{\partial n_a} = \mathrm{i}\rho_a \omega v_a, \tag{8}$$

whereas the porous foam is assumed to be in contact with rigid walls. To simulate the case of foam which is bonded to the wall, we require that

$$\boldsymbol{u} = 0, \tag{9}$$

$$U_n - u_n = 0. \tag{10}$$

In the case where the foam is sliding the above condition holds for the normal component only and the tangential stress must be set to zero,

$$(\boldsymbol{\sigma n}_p) \cdot \boldsymbol{t} = 0, \tag{11}$$

$$U_n = u_n = 0. \tag{12}$$

B. Variational formulation

The starting point is to combine the weak integral formulations for the mixed formulation (2), (3), and the Helmholtz equation (1). This gives

$$\begin{aligned}
&\int_{V_p} (\boldsymbol{\sigma}^s : \delta\varepsilon - \rho\omega^2 \boldsymbol{u} \cdot \delta\boldsymbol{u})\,\mathrm{d}V \\
&+\int_{V_p} \left(\frac{\phi^2}{\omega^2 \rho_{22}} \nabla p_p \cdot \nabla \delta p_p - \frac{\phi^2}{R} p_p \delta p_p \right) \mathrm{d}V \\
&-\int_{V_p} \frac{\phi}{\tilde{\alpha}} \delta(\nabla p_p \cdot \boldsymbol{u})\,\mathrm{d}V - \int_{V_p} \left[\phi \left(1 + \frac{Q}{R} \right) \right] \delta(p_p \nabla \cdot \boldsymbol{u})\,\mathrm{d}V \\
&+\int_{V_p} \left(\frac{1}{\rho_a \omega^2} \nabla p_a \cdot \nabla \delta p_a - \frac{1}{\rho_a c_a^2} p_a\, \delta p_a \right) \mathrm{d}V \\
&+I_c + I_p^{\mathrm{bo}} + I_p^{\mathrm{sl}} = \mathrm{i}\rho_a \omega \int_{S_a} v_a\, \delta p_a\,\mathrm{d}S,
\end{aligned} \tag{13}$$

where the dynamic tortuosity $\tilde{\alpha}$ is obtained from $\phi/\tilde{\alpha} = \gamma + \phi(1 + Q/R)$. Here I_c, I_p^{bo}, and I_p^{sl} stand for the boundary integral terms arising from integration by parts. Using a conventional nodal-based element, their explicit form can be found in Ref. 5. The type of approximation considered in this work involves global coefficients so transmission conditions and boundary conditions must be enforced using Lagrange multipliers. This is now explicitly stated:

(1) The air-porous interface S_c. It is convenient to introduce a Lagrange multiplier defined as the normal derivative of the acoustic pressure at the air-porous interface. To be more precise we put

$$\lambda = \frac{1}{\rho_a \omega^2} \frac{\partial p_a}{\partial n_p}. \tag{14}$$

After applying the continuity conditions (5), we find[5]

$$I_c = \int_{S_c} \delta(p_p\, u_n)\,\mathrm{d}S + \int_{S_c} \lambda(\delta p_a - \delta p_p)\,\mathrm{d}S. \tag{15}$$

Note the last integral in Eq. (15) does not appear in Ref. 5 as the continuity of pressure (i.e., $p_p = p_a$ and $\delta p_p = \delta p_a$) between the two domains is simply taken into account algebraically through assembling. In the PUFEM formulation, this condition must be enforced weakly as

$$\int_{S_c} \delta\lambda(p_a - p_p)\,\mathrm{d}S = 0. \tag{16}$$

(2) The bonding conditions at the wall S_p^{bo}. Here we introduce a Lagrange multiplier (in a vector form) which comprises the stress components at the hard wall, i.e., $\boldsymbol{\lambda}^{\mathrm{bo}} = \boldsymbol{\sigma n}_p$. The boundary integral reads

$$I_p^{\mathrm{bo}} = \int_{S_p^{\mathrm{bo}}} \boldsymbol{\lambda}^{\mathrm{bo}} \cdot \delta\boldsymbol{u}\,\mathrm{d}S. \tag{17}$$

The condition that the elastic phase displacement must be zero at the wall is enforced weakly,

$$\int_{S_p^{\mathrm{bo}}} \delta\boldsymbol{\lambda}^{\mathrm{bo}} \cdot \boldsymbol{u}\,\mathrm{d}S = 0. \tag{18}$$

(3) The sliding conditions on S_p^{sl}. Here only the normal displacement must be set to zero and by defining $\lambda^{\mathrm{sl}} = (\boldsymbol{\sigma n}_p) \cdot \boldsymbol{n}_p$, the boundary integral becomes

$$I_p^{\mathrm{sl}} = \int_{S_p^{\mathrm{sl}}} \lambda^{\mathrm{sl}} \delta u_n\,\mathrm{d}S, \tag{19}$$

with the additional constraints

$$\int_{S_p^{\mathrm{sl}}} \delta\lambda^{\mathrm{sl}} u_n\,\mathrm{d}S = 0. \tag{20}$$

Before we end this section, we may notice that the PUFEM weak formulation yields a symmetric matrix (but with complex coefficients) as in conventional nodal-based elements. The final system can always be recast as the general form given by Eq. (19) in Ref. 36.

C. Plane wave finite elements

Let the domain V be partitioned into L non-overlapping subdomains $V^{(l)}$ where l ranges from 1 to L. Each sub-domain, or finite element in the engineering terminology, is defined via the geometric mapping $\boldsymbol{r} = \boldsymbol{r}^{(l)}(\xi, \eta)$ between the real space and the local system of triangular type,

$$\mathcal{T} = \{\xi \geq 0, \eta \geq 0, \xi + \eta \leq 1\}.$$

The key ingredient of the PUFEM relies on the enrichment of the conventional finite element approximation by including solutions of the homogeneous partial differential

equation.[20,40–42] In this work, we favored the use of plane waves as these are easily computed. In each sub-domain $V^{(l)}$ belonging to the acoustic domain, the acoustic pressure is expanded as

$$p_a(\boldsymbol{r}) = \sum_{j=1}^{3}\sum_{q=1}^{Q_j} N_j^3(\xi,\eta)\exp\left(\mathrm{i}k_a\,\boldsymbol{d}_{jq}\cdot(\boldsymbol{r}-\boldsymbol{r}_j^{(l)})\right)P_{a,jq}^{(l)}, \tag{21}$$

where the plane wave amplitudes $P_{a,jq}^{(l)}$ are unknown coefficients and functions N_j^3 are the classical linear shape functions on triangular elements. Points $\boldsymbol{r}_j^{(l)}$ are the three nodes associated with element $V^{(l)}$. Their presence in Eq. (21) ensures that the nodal values are recovered simply as

$$p_a(\boldsymbol{r}_j^{(l)}) = \sum_{q=1}^{Q_j} P_{a,jq}^{(l)}, \tag{22}$$

and that the element matrices associated with this oscillatory basis do not become artificially either too big or too small (note this problem is not encountered with real wavenumbers). The directions, attached to node j, are chosen to be evenly distributed over the unit circle; that is

$$\boldsymbol{d}_{jq} = (\cos(\theta_q),\sin(\theta_q)) \quad \text{where} \quad \theta_q = \frac{2\pi q}{Q_j},$$
$$q = 1,\ldots,Q_j. \tag{23}$$

The number of plane waves attached to each node $j=1,2,3$ must be dependent on the frequency and the element size. Although there is no rigorous theory in this matter as this number might also depend on the studied configuration, there is a common acceptance that the following criteria should provide a good estimate:[43]

$$Q_j = \mathrm{round}\,[k_a h + C(k_a h)^{1/3}]. \tag{24}$$

Here, h is taken as the largest element edge length connected to node j within the acoustic domain and the constant C is usually chosen to lie in the interval $C\in[2,20]$. This coefficient can be adjusted depending on the configuration and the expected accuracy. Note that Eq. (24) is restricted to two-dimensional domains only. In the poroelastic domain, the plane wave decomposition for the solid phase displacement is obtained by recalling that $\boldsymbol{u}$ admits the Helmholtz decomposition $\boldsymbol{u} = \nabla(\varphi_1+\varphi_2)+\nabla^{\perp}\varphi_3$. Under this form, each potential φ_α, $(\alpha=1,2,3)$ fulfills the Helmholtz equation

$$\Delta\varphi_\alpha + k_\alpha^2\varphi_\alpha = 0. \tag{25}$$

Here, complex-valued wavenumbers k_α are given explicitly as[2]

$$k_1^2 = \frac{\omega^2}{2(PR-Q^2)}(P\rho_{22}+R\rho_{11}-2Q\rho_{12}+\sqrt{\Delta}), \tag{26}$$

$$k_2^2 = \frac{\omega^2}{2(PR-Q^2)}(P\rho_{22}+R\rho_{11}-2Q\rho_{12}-\sqrt{\Delta}), \tag{27}$$

$$k_3^2 = \frac{\omega^2}{N}\left(\frac{\rho_{11}\rho_{22}-\rho_{12}^2}{\rho_{22}}\right), \tag{28}$$

with $P=A+2N$ and

$$\Delta = (P\rho_{22}+R\rho_{11}-2Q\rho_{12})^2 - 4(PR-Q^2)(\rho_{11}\rho_{22}-\rho_{12}^2). \tag{29}$$

This invites us to consider the following finite element plane wave approximation as

$$\begin{aligned}\boldsymbol{u}(\boldsymbol{r}) = &\sum_{\alpha=1}^{2}\sum_{j=1}^{3}\sum_{q=1}^{Q_{\alpha,j}} N_j^3(\xi,\eta)\,\boldsymbol{d}_{\alpha,jq} \\ &\times\exp\left(\mathrm{i}k_\alpha d_{\alpha,jq}\cdot(\boldsymbol{r}-\boldsymbol{r}_j^{(l)})\right)U_{\alpha,jq}^{(l)} \\ &+\sum_{j=1}^{3}\sum_{q=1}^{Q_{3,j}} N_j^3(\xi,\eta)\,\boldsymbol{d}_{3,jq}^{\perp} \\ &\times\exp(\mathrm{i}k_3\boldsymbol{d}_{3,jq}\cdot(\boldsymbol{r}-\boldsymbol{r}_j^{(l)}))U_{3,jq}^{(l)}.\end{aligned} \tag{30}$$

The wave directions are chosen as in Eq. (23), i.e.,

$$\boldsymbol{d}_{\alpha,jq} = (\cos(\theta_q),\sin(\theta_q)) \quad \text{where} \quad \theta_q = \frac{2\pi q}{Q_{\alpha,j}},$$
$$q = 1,\ldots,Q_{\alpha,j}, \quad \alpha = 1,2,3. \tag{31}$$

As for the number of wave directions, the same criteria is applied with the real part of the wavenumber since it corresponds to the oscillating part of the solution

$$Q_{\alpha,j} = \mathrm{round}\,[\mathrm{Re}(k_\alpha)h + C(\mathrm{Re}(k_\alpha)h)^{1/3}]. \tag{32}$$

Similarly, h is taken as the largest element edge length connected to node j within the poroelastic domain. Following Ref. 2, the pore pressure can be written as a linear combination of φ_1 and φ_2 and in fact

$$-\phi p_p = (Q+R\mu_1)\Delta\varphi_1 + (Q+R\mu_2)\,\Delta\varphi_2, \tag{33}$$

where μ_1 and μ_2 are the wave amplitude ratios between the two phases in the porous material.[2] Thus, it is natural to consider the following plane wave expansion for the pressure using the longitudinal waves only:

$$\begin{aligned}p_p(\boldsymbol{r}) = &\sum_{\alpha=1}^{2}\sum_{j=1}^{3}\sum_{q=1}^{Q_{\alpha,j}} N_j^3(\xi,\eta) \\ &\times\exp\left(\mathrm{i}k_\alpha d_{\alpha,jq}\cdot(\boldsymbol{r}-\boldsymbol{r}_j^{(l)})\right)P_{\alpha,jq}^{(l)}.\end{aligned} \tag{34}$$

In the present work, the finite element geometries are defined using standard quadratic shape functions on triangular elements

$$\boldsymbol{r}^{(l)}(\xi,\eta) = \sum_{j=1}^{6} N_j^6(\xi,\eta)\boldsymbol{r}_j^{(0)}, \tag{35}$$

as this description is integrated in most software (here the finite element mesh generator Gmsh is used[44]). In

Eq. (35) extra nodes $\boldsymbol{r}_j^{(l)}$ for $j = 4, 5, 6$ correspond to the mid-node of the edges as shown in Fig. 2. On both sides of the air-porous interface, meshes are designed to be compatible. This choice is made for practical reasons as it considerably eases the numerical implementation of the method. At the matching interface, the Lagrange multiplier is expanded using real plane waves with the highest oscillations, i.e.,

$$\mathrm{Re}(k_{\bar{\alpha}}) = \max_{\alpha} (\mathrm{Re}(k_\alpha)), \tag{36}$$

that is

$$\lambda(\boldsymbol{r}) = \sum_{j=1}^{2} \sum_{q=1}^{Q_{\bar{\alpha},j}} N_j^2(\xi) \exp(\mathrm{i}k_{\bar{\alpha}} \boldsymbol{d}_{\bar{\alpha},jq} \cdot (\boldsymbol{r} - \boldsymbol{r}_j^{(l)})) \lambda_{jq}^{(l)}, \tag{37}$$

where amplitudes $\lambda_{jq}^{(l)}$ are unknown coefficients, linear functions N_j^2 are simply the restriction of the shape functions N_j^3 on the boundary line S_c, and the superscript (l) refers to the adjacent element $V^{(l)}$ belonging to the porous domain. The other multipliers corresponding to the stress components at the hard wall are approximated using a similar expansion.

Finally, the element matrices are formed using a Galerkin scheme: the weight functions δp_a, δp_p, $\delta \boldsymbol{u}$, etc…, are chosen from the plane wave basis Eqs. (21), (34), (30), and (37). As plane wave finite elements may span many wavelengths, the computation of the element matrices requires the integration of highly oscillating functions, especially in the porous domain where the real part of the wavenumber can be much larger than the acoustic one. Here, the adaptive Gauss quadrature algorithm `gauleg` from Numerical Recipes[45] is used, and the integration over the triangular domain $\mathcal{T}$ is carried out by general Cartesian product rules as in Ref. 21. The number of Gauss points is chosen to ensure that at least an average of 20 points per wavelength (the smallest one is considered in the porous domain) are used in the computation. As the examples will show in Sec. IV, this number might need to be increased to achieve better accuracy.

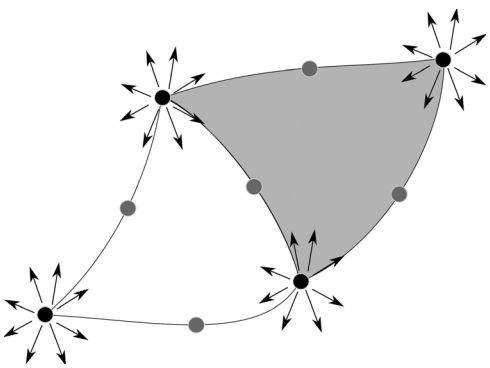

FIG. 2. Plane wave finite element with quadratic geometry and matching mesh.

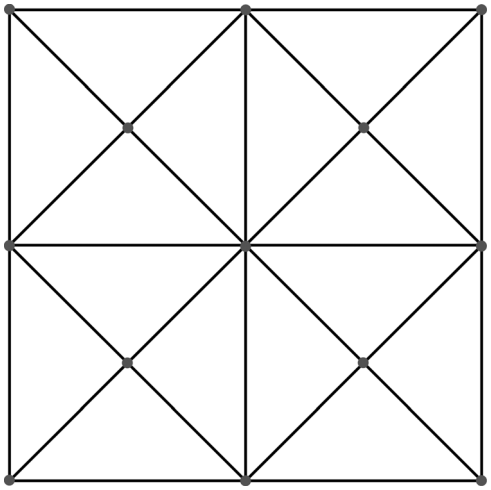

FIG. 3. Tested mesh for the porous domain.

III. PUFEM PERFORMANCES FOR THE POROELASTIC WAVE EQUATIONS

The aim of this section is to assess the PUFEM performances for the discretization of the poroelastic wave equations only. Our main concern is to identify the gain of the present method in terms of data reduction when compared to classical FEM discretization schemes.[9] The porous domain has the shape of a square of size 0.2 m which is partitioned into 16 identical PUFEM elements as shown in Fig. 3. The origin corresponds to the bottom left corner of the mesh. In all numerical tests presented in this work, the XFM foam whose properties are reported in Table I was chosen. An exact poroelastic wave field $\boldsymbol{u}^{ex.}$ and $p_p^{ex.}$ can be constructed via the Helmholtz decomposition and Eq. (34) from the three potentials $\varphi_\alpha^{ex.}$ $(\alpha = 1, 2, 3)$ each having the form of a traveling plane wave,

$$\varphi_\alpha^{ex.} = \frac{1}{|k_\alpha|} \exp(\mathrm{i}k_\alpha \boldsymbol{d}_\alpha \cdot (\boldsymbol{r} - \boldsymbol{r}^0)). \tag{38}$$

Here, the reference point $\boldsymbol{r}^0 = (0.1, 0.1)$ is the center of the square domain and the directions of propagation $\boldsymbol{d}_\alpha = (\cos(\theta_\alpha), \sin(\theta_\alpha))$ are chosen to be $\theta_1 = \sqrt{2}\pi$, $\theta_2 = \sqrt{3}\pi$, and $\theta_3 = \sqrt{5}\pi$.

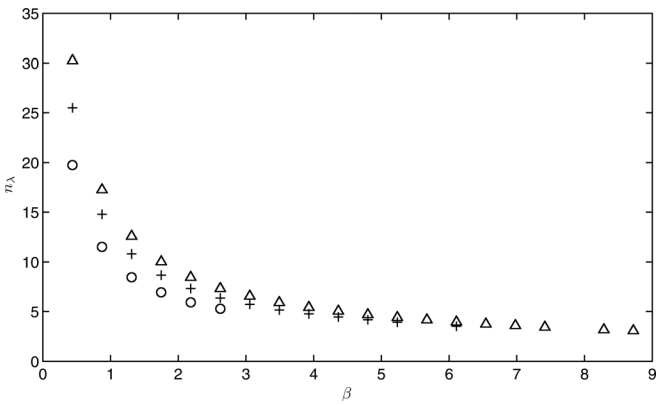

FIG. 4. Efficiency of the PUFEM for the poroelastic wave equations; $C = 5$ (circle), $C = 10$ (cross), $C = 15$ (triangle).

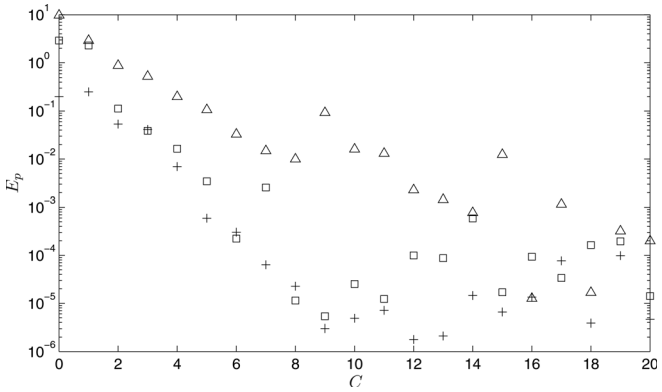

FIG. 5. Convergence study for the pressure; $f = 100$ Hz (cross), $f = 1000$ Hz (square), $f = 5000$ Hz (triangle).

This choice was motivated to ensure that none of the directions in the PUFEM plane wave basis coincide with those of the exact field. Because this is not a poroelastic-acoustic coupled problem but rather an artificial one, the boundary terms arising from the weak formulation of the poroelastic wave equations are all known, this yields (once placed in the right-hand side of the equation)

$$\int_{S_p} \boldsymbol{\sigma}^{ex.} \boldsymbol{n}_p \cdot \delta \boldsymbol{u} \, \mathrm{d}S + \int_{S_p} \phi (U_n^{ex.} - u_n^{ex}) \delta p_p \, \mathrm{d}S. \tag{39}$$

It is convenient for the analysis to assess the efficiency of the method by defining the average discretization level n_λ defined as the average number of variables needed to capture a single wavelength,

$$n_\lambda = \lambda_{\bar{\alpha}} \sqrt{\frac{N_{\mathrm{dof}}}{\mathrm{area}\,(V_p)}}, \tag{40}$$

where N_{dof} is the total number of degrees of freedom. In Eq. (40), it is understood that $\lambda_{\bar{\alpha}} = 2\pi/\mathrm{Re}(k_{\bar{\alpha}})$ where the index $\bar{\alpha}$ corresponds to the wave type having the highest oscillation, see Eq. (36). For instance, using conventional finite element discretization, it is widely accepted that numerical solutions of the Helmholtz equation are expected to be of acceptable accuracy if around ten nodes per wavelength are used. This condition is however difficult to establish for the poroelastic wave equations depending on the type of waves which is predominant in the porous material and/or the boundary conditions.[9] Another important parameter is the size of the PUFEM element and more precisely the number of (smallest) wavelengths spanning over a characteristic element length h_{mesh} of the finite element mesh which we shall define as

$$\beta = \frac{h_{\mathrm{mesh}}}{\lambda_{\bar{\alpha}}}. \tag{41}$$

By varying the frequency, the dependence between the discretization level n_λ, the element length (in β), and the coefficient C which defines the number of plane waves at each node is conveniently reported in Fig. 4. Here, all symbols correspond to numerical results obtained with less than 1% deviation (for both p and $\boldsymbol{u}$) compared with the exact solution. The mean error for the pressure and for the displacement is measured using

$$E_p = 100 \times \frac{\|p - p^{ex.}\|}{\|p^{ex.}\|} \quad \text{and} \quad E_u = 100 \times \frac{\|\boldsymbol{u} - \boldsymbol{u}^{ex.}\|}{\|\boldsymbol{u}^{ex.}\|}, \tag{42}$$

where p stands for either the pore pressure or the acoustic pressure and $\|\cdot\|$ stands for the classical L_2-norm with respect to the domain under consideration.

Figure 4 shows typical L-shaped curves similar to previous studies. This behavior can be anticipated in the case of an ideal mesh of infinite extent for the Helmholtz equation.[36] In this particular case, it can be shown that the average discretization level decreases like $\mathcal{O}(1/\sqrt{\beta})$. This somewhat surprising fact is simply reflected in the formula (24) indicating that the number of variables needed to simulate

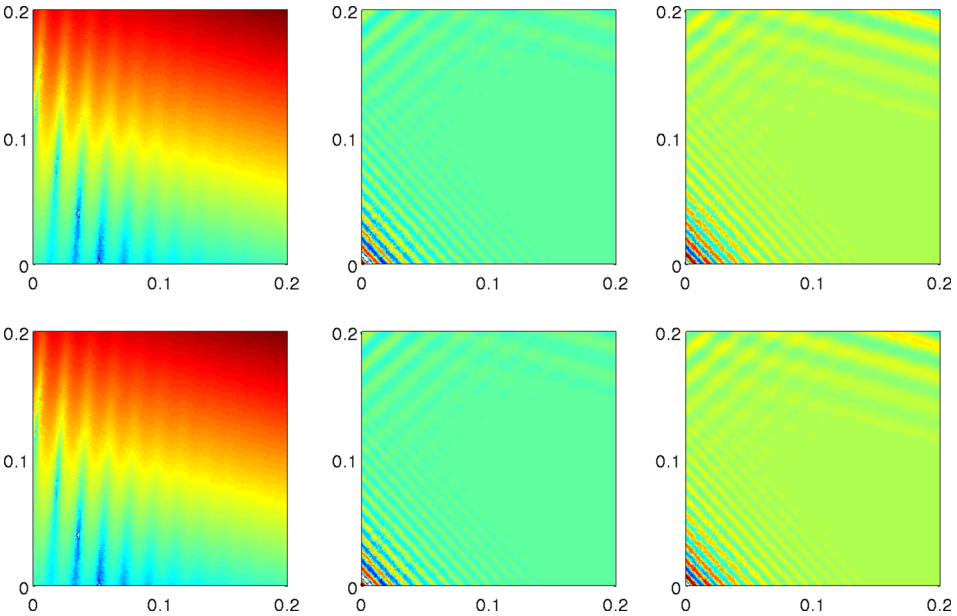

FIG. 6. (Color online) Poroelastic wave field (real part) over the computational domain. Top: Computed, bottom: Exact. From left to right: Acoustic pressure (p_p), horizontal displacement (u_x), and vertical displacement (u_y).

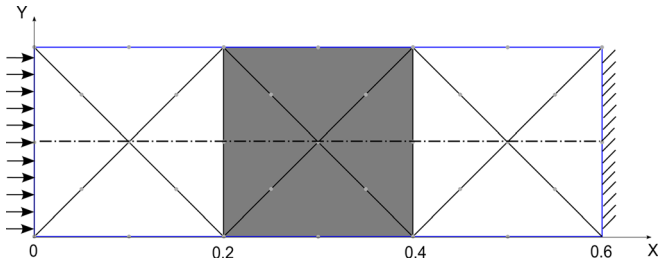

FIG. 7. (Color online) The standing wave tube; the gray color refers to the porous material.

approximately β^2 wavelengths over a bi-dimensional domain behaves almost linearly with respect to β. Results of Fig. 4 show that this behavior is also observed for the poroelastic wave equations. We can anticipate that standard FEM would require a discretization level of at least $n_\lambda \approx 20$; this figure is based on 6 degrees of freedom per smallest wavelength and per independent variables, namely p_p, u_x, and u_y. Clearly, for high frequency or equivalently for large PUFEM elements, the gain is substantial as very accurate results can be obtained with less than 5 degrees of freedom per wavelength, and the gain would be even greater in three dimensions. In this respect, it should be noticed that the error on the pressure is usually much lower than the error on the displacement, say by an order of magnitude at least. This can be explained by the absence of the shortest wavelength; that is the shear wave, in the expression for the pressure. The other reason lies in the nature of the mixed ($\boldsymbol{u}$, p_p) formulation for which it is known that both physical variables do not converge at the same rate and the order of approximation for the displacement must be higher than for the pressure; this is discussed for instance in Ref. 7.

Figure 5 shows a convergence study for the pore pressure in the computational domain. As the total number of degrees of freedom is solely defined via the coefficient C in Eqs. (24) and (32), it is natural and instructive to carry out the convergence analysis with respect to this single coefficient. This confirms that the selection rule [Eqs. (24) and (32)] which was originally devised for the non-dissipative Helmholtz equation[43] performs very well when applied to poroelastic equations (note this excellent accuracy was obtained by taking 20 integration points per wavelength). Again, this level of accuracy would be literally impossible to reach with conventional nodal-based elements. We can observe that the convergence (with respect to C) is a little slower for higher frequencies. This suggests that the tuning coefficient C might be weakly dependent on kh. The

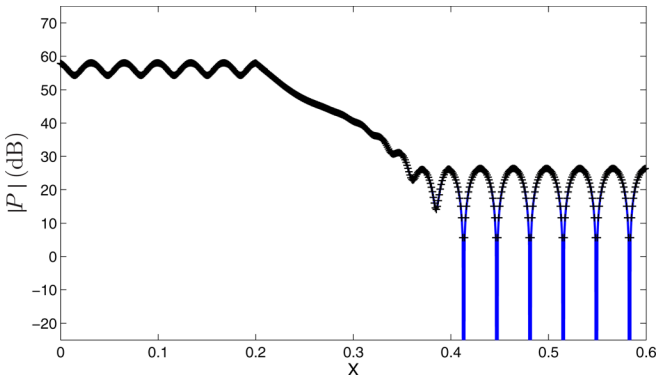

FIG. 8. (Color online) The standing wave tube: Pressure level (in dB) along the tube (sliding foam). Solid line: Analytical results; Markers: Numerical results obtained with the PUFEM.

fact that C must be increased at high frequency in order to maintain the same accuracy is also reflected in Fig. 4. Now, the somewhat erratic behavior of the convergence curves when C increases is due to the ill-conditioning nature of the PUFEM with plane waves combined with the mixed ($\boldsymbol{u}$, p_p) formulation which is also known to be ill-conditioned even for finite element low-order approximations. As far as the authors' experience, the conditioning issue is not necessarily a major problem as long as the matrices are calculated with sufficient precision in order to avoid results corrupted by round-off errors during the inversion process.

For the sake of illustration, Fig. 6 (left) shows the sound pressure level (in dB) calculated as well as the exact solution at 10 000 Hz. The real part of the horizontal and vertical displacements is also shown. In this example, the number of smallest wavelengths spanning a single PUFEM element can be identified (around five) so the gain in terms of data reduction, is quite substantial. In this specific example, the three wavenumbers are $k_1 = 271.4 + 31.98\text{i}$, $k_2 = 380.6 + 27.05\text{i}$, and $k_3 = 774.9 + 40.14\text{i}$. The number of plane waves attached to each interior node of the mesh is calculated according to Eq. (33) (with $C = 15$) giving $Q_1 = 72$, $Q_2 = 90$, and $Q_3 = 142$.

IV. EXTENSION TO POROELASTIC-ACOUSTIC PROBLEMS

A. The standing wave tube

In order to measure precisely the performance of the PUFEM for the simulation of poroelastic-acoustic problems,

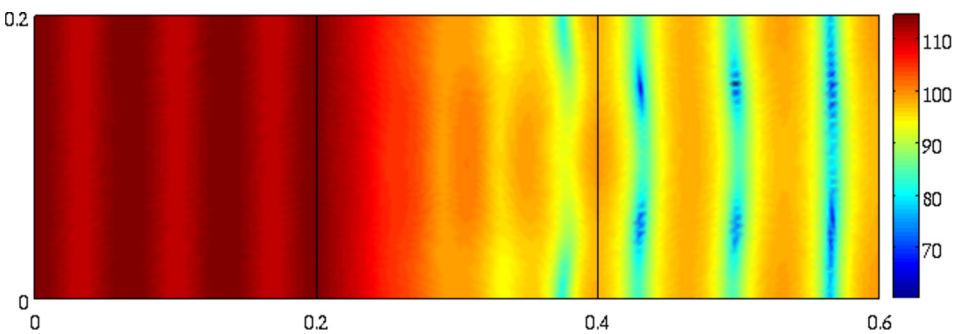

FIG. 9. (Color online) The standing wave tube: Pressure level (in dB) along the tube (foam bonded to the wall).

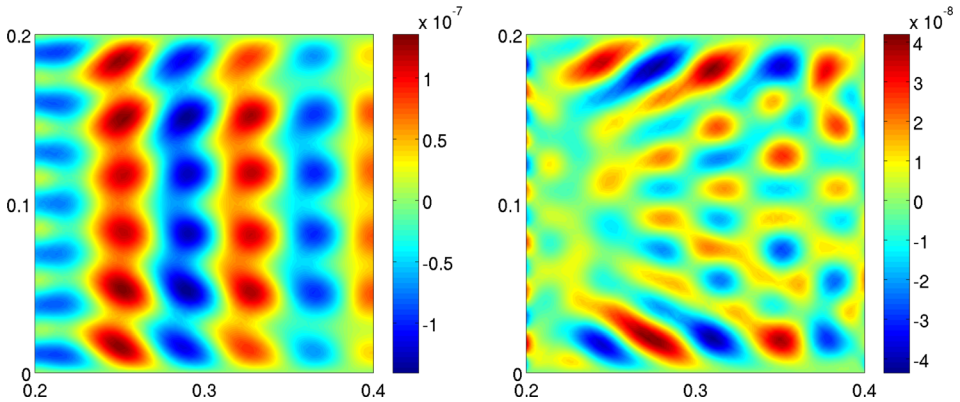

FIG. 10. (Color online) The standing wave tube: elastic displacement fields (real part) in both x and y directions (foam bonded to the wall).

the first series of tests concerns that of a standing wave tube whose geometry is illustrated in Fig. 7. The triangular mesh used in our calculation is also shown. The tube of length $L = 0.6$ m is divided into three regions of equal length with $x_1 = L/3$ and $x_2 = 2L/3$. The first region contains the incident and reflected wave and a normal velocity is imposed at the left wall. The second area in gray is the porous absorber which, for the moment, is allowed to slide tangentially to the wall. The last region is an air gap terminated by a rigid wall. This simple test case is chosen as one-dimensional analytical solutions are easily obtained (see the Appendix) and it corresponds to configurations of practical interest.[28] As the exact solution can be expressed as the sum of two horizontal plane waves propagating in opposite directions, all calculations were performed without the horizontal directions in order to ensure that the exact solution is not included in the plane wave basis. For this configuration, the characteristic length of the mesh is the longest edge, that is $h_{\text{mesh}} = 0.2$ m which also corresponds to the width of the tube. The graph of the acoustic pressure (in dB) with respect to the horizontal axis is shown in Fig. 8 for the XFM foam. These results correspond to a relatively high frequency calculation with $f = 5000$ Hz. The comparison with the analytical curve, in a solid line, shows very good agreements as discrepancies are hardly noticeable. Note that in the third region (air gap), where the sound level is extremely low, results are accurate within 1% whereas the error level reaches about 5×10^{-7}% in the first region! These results are computed by taking $C = 15$ which yields around 5300 degrees of freedom. They show a sound transmission loss of about 40 up to 60 dB between the incident and the silent zone. For the sake of comparison with FEM, a series of numerical tests have been carried out using standard quadratic interpolation for both displacements and pressure. It was found that reasonable results, say below 3% of errors, can be obtained with approximately 16 000 degrees of freedom. Here the gain in terms of data reduction is not drastic. This is due to the finiteness of the domain, i.e., the contribution of the plane wave basis associated with nodes on the boundary is restricted to the interior domain, the relatively small number of elements, and the additional number of degrees of freedom (the Lagrange multiplier) at the air-porous interfaces and at the wall. In the last example, the foam is sliding so the shear wave component ($\alpha = 3$) as well as the vertical displacement are absent. In a second test case, we increase the difficulty by considering porous foam which is now bonded to the wall. Figure 9 shows the resulting pressure field level (in dB) over the whole computational domain at a frequency of 2500 Hz. The associated elastic displacement fields in both x and y directions are also displayed in Fig. 10. For this example, the integration procedure was pushed to around 30 Gauss points per wavelength to ensure that convergence was reached. The number of plane waves attached at each node (except the middle one) in the porous domain is $Q_1 = 76$, $Q_2 = 90$, and $Q_3 = 142$. Here there are approximately 3 to 4 oscillations per element.

B. Applications

In the last example, the PUFEM is applied to the numerical simulation of the sound field in a bi-dimensional interior car cavity. The geometry and the PUFEM mesh used in our calculation is shown in Fig. 11, the length of the car is about 3.2 m. The sound field is generated by imposing an arbitrary normal velocity at the front windscreen (we simply put $\partial p_a/\partial n_a = 1$). The car seat, in gray color, is made of poroelastic foam (XFM). In Fig. 12 are shown the distribution of sound in the car cavity at a frequency of 5000 Hz. Note the

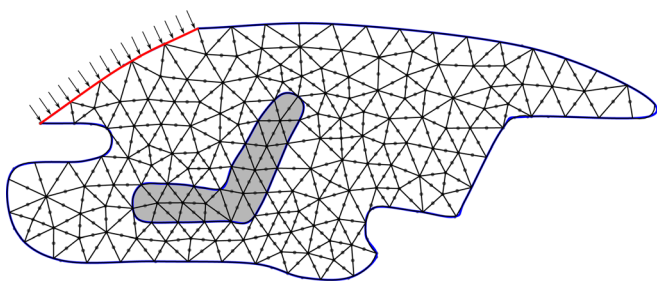

FIG. 11. (Color online) Model of bi-dimensional car interior cavity with the PUFEM mesh.

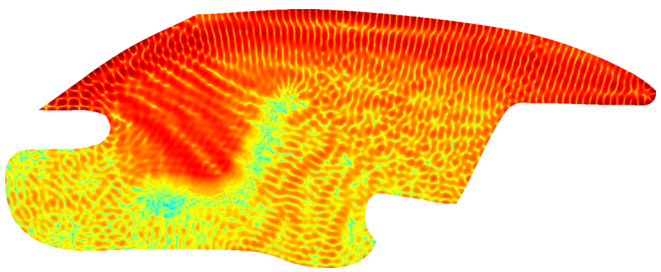

FIG. 12. (Color online) Sound pressure level (in dB) in the car at 5000 Hz.

PUFEM convergence was reached using $C=20$ and the computation of the element matrices was performed using 40 integration points per wavelength. The total number of degrees of freedom including the Lagrange multipliers is 27 988. A similar calculation using standard quadratic finite elements would require about 150 000 variables to achieve the same accuracy. This rough estimation is based on previous studies led by the authors.[36]

V. CONCLUSIONS

This paper has demonstrated the applicability of the PUFEM for the numerical simulation of elastic and pressure waves in poroelastic media. The main ingredient of the method relies on the enrichment of the conventional finite element approximation by including a set of plane waves propagating in various directions. The performances of the method, measured in terms of data reduction, are assessed for an artificial problem for which analytical solutions are available. It is shown that the PUFEM allows a substantial reduction of the number of degrees of freedom compared to the standard FEM and that best performances are obtained when the element size contains a minimum of three to five wavelengths (here the shortest wavelength is considered). To show the interest of the method for tackling problems of practical interests the PUFEM is extended to the analysis of poroelastic-acoustic problems in Sec. IV. Coupling conditions at the air-porous interface as well as fixed or sliding edge conditions are presented and numerically tested. It is shown that the technique is a good candidate for solving noise control problems at medium and high frequency. Finally, it is hoped that this work could serve as a starting point for the analysis of tri-dimensional short wave problems involving poroelastic materials with potential applications, not only in acoustics, but also in geophysics, ultrasonic, and seismic modeling. In this regard, the reader may find interesting references in this topic in a recent review.[46]

APPENDIX: SOLUTION OF THE STANDING WAVE TUBE

Here are presented the guidelines for the one-dimensional solution of the standing wave tube described in Sec. IV. For a brief nomenclature, the indices $i=$ I, II, III is associated with the three regions $x \in [0, L/3]$, $x \in [L/3, 2L/3]$, and $x \in [2L/3, L]$. In the air domain (i.e., $i=$ I and III), the acoustic displacement potential φ_0^i can be written as the sum of two traveling plane waves,

$$\varphi_0^i = A_0^{i,+} e^{ik_a x} + A_0^{i,-} e^{-ik_a x}. \tag{A1}$$

The acoustic pressure and the horizontal displacement in each region is obtained from $p_a^i = \omega^2 \rho_a \varphi_0$ and $w_x^i = \partial_x \varphi_0$. In the poroelastic domain, there is no shear component and the displacements are horizontal only. By using the Helmholtz decomposition, we have[2]

$$u_x = \partial_x \varphi_1^{\mathrm{II}} + \partial_x \varphi_2^{\mathrm{II}}, \tag{A2}$$

$$U_x = \mu_1 \partial_x \varphi_1^{\mathrm{II}} + \mu_2 \partial_x \varphi_2^{\mathrm{II}}, \tag{A3}$$

where μ_1 and μ_2 are the wave amplitude ratios between the two phases in the porous material.[2] Here, each potential ($\alpha=1, 2$) has the form

$$\varphi_\alpha^{\mathrm{II}} = A_\alpha^{\mathrm{II},+} e^{ik_\alpha x} + A_\alpha^{\mathrm{II},-} e^{-ik_\alpha x}. \tag{A4}$$

The normal total stress is obtained thanks to Eq. (4),

$$\sigma_{xx} = -\varphi_1^{\mathrm{II}} k_1^2 [(P+Q) + \mu_1 (R+Q)] - \varphi_2^{\mathrm{II}} k_2^2 [(P+Q) + \mu_2 (R+Q)], \tag{A5}$$

and similarly, using Eq. (34),

$$p_p = \frac{1}{\phi} [(Q + \mu_1 R) \varphi_1^{\mathrm{II}} k_1^2 + (Q + \mu_2 R) \varphi_2^{\mathrm{II}} k_2^2]. \tag{A6}$$

Once the acoustic velocity is prescribed at $x=0$, the coupling conditions (5), (6), and (7) at the air-porous interface at $x_1 = L/3$ and $x_2 = L/3$ as well as the wall boundary condition at $x=L$ yield a matrix system for the 8 unknown plane waves amplitudes $A_\alpha^{i,\pm}$.

[1] M. Aretz and M. Vorländer, "Efficient modeling of absorbing boundaries in room acoustic fe simulations," Acta Acust. Acust. **96**, 1042–1050 (2010).
[2] J. Allard and N. Atalla, *Propagation of Sound in Porous Media: Modelling Sound Absorbing Materials*, 2nd revised ed. [Wiley-Blackwell (an imprint of John Wiley and Sons Ltd.), London, 2009], 372 pp.
[3] R. Panneton and N. Atalla, "An efficient finite element scheme for solving the three-dimensional poroelasticity problem in acoustics," J. Acoust. Soc. Am. **101**, 3287–3298 (1997).
[4] N. Atalla, R. Panneton, and P. Debergue, "A mixed displacement-pressure formulation for poroelastic materials," J. Acoust. Soc. Am. **104**, 1444–1452 (1998).
[5] N. Atalla, M. A. Hamdi, and R. Panneton, "Enhanced weak integral formulation for the mixed (u,p) poroelastic equations," J. Acoust. Soc. Am. **109**, 3065–3068 (2001).
[6] O. Dazel and N. Dauchez, "The Finite Element Method for porous materials," in *Materials and Acoustics Handbook*, edited by M. Bruneau and C. Potel (John Wiley and Sons Ltd., London, 2009), Chap. 12, pp. 327–338.
[7] B. Nennig, M. Ben Tahar, and E. Perrey-Debain, "A displacement-pressure finite element formulation for analyzing the sound transmission in ducted shear flows with finite poroelastic lining," J. Acoust. Soc. Am. **130**, 42–51 (2011).
[8] S. Rigobert, N. Atalla, and F. Sgard, "Investigation of the convergence of the mixed displacement-pressure formulation for three-dimensional poroelastic materials using hierarchical elements," J. Acoust. Soc. Am. **114**, 2607–2617 (2003).
[9] N. Dauchez, S. Sahraoui, and N. Atalla, "Convergence of poroelastic finite elements based on Biot displacement formulation," J. Acoust. Soc. Am. **109**, 33–40 (2001).
[10] N.-E. Hörlin, M. Nordström, and P. Göransson, "A 3-D hierarchical FE formulation of Biots equations for elasto-acoustic modelling of porous media," J. Sound Vib. **245**, 633–652 (2001).
[11] N.-E. Hörlin, "3D hierarchical HP-FEM applied to elasto-acoustic modelling of layered porous media," J. Sound Vib. **285**, 341–363 (2005).
[12] O. Dazel, F. Sgard, C.-H. Lamarque, and N. Atalla, "An extension of complex modes for the resolution of finite-element poroelastic problems," J. Sound Vib. **253**, 421–445 (2002).
[13] O. Dazel, F. Sgard, and C.-H. Lamarque, "Application of generalized complex modes to the calculation of the forced response of three-dimensional poroelastic materials," J. Sound Vib. **268**, 555–580 (2003).
[14] O. Dazel, B. Brouard, N. Dauchez, and A. Geslain, "Enhanced Biot's finite element displacement formulation for porous materials and original resolution methods based on normal modes," Acta Acust. Acust. **95**, 527–538 (2009).
[15] R. Rumpler, J.-F. Deü, and P. Göransson, "Application of generalized complex modes to the calculation of the forced response of the three-

dimensional poroelastic materials," J. Acoust. Soc. Am. **132**, 3162–3179 (2012).
[16]P. Davidsson and G. Sandberg, "A reduction method for structure-acoustic and poroelastic-acoustic problems using interface-dependent Lanczos vectors," Comput. Methods Appl. Mech. Eng. **195**, 1933–1945 (2006).
[17]O. Tanneau, P. Lamary, and Y. Chevalier, "A boundary element method for porous media," J. Acoust. Soc. Am. **120**, 1239–1250 (2006).
[18]J.-D. Chazot, B. Nennig, and E. Perrey-Debain, "Harmonic response computation of poroelastic multilayered structures using ZPST shell elements," Comput. Struct. **121**, 99–107 (2013).
[19]P. Bettess, "Short wave scattering: Problems and techniques," Philos. Trans. R. Soc. London, Ser. A **362**, 421–443 (2004).
[20]J. Melenk and I. Babuška, "The partition of unity finite element method. Basic theory and applications," Comput. Methods Appl. Mech. Eng. **139**, 289–314 (1996).
[21]E. Perrey-Debain, O. Laghrouche, P. Bettess, and J. Trevelyan, "Plane wave basis finite elements and boundary elements for three-dimensional wave scattering," Philos. Trans. R. Soc. London, Ser. A **362**, 561–577 (2004).
[22]O. Cessenat and B. Després, "Application of an ultraweak variational formulation of elliptic pdes to the two-dimensional Helmholtz problem," SIAM (Soc. Ind. Appl. Math.) J. Numer. Anal. **35**, 255–299 (1998).
[23]T. Huttunen, P. Monk, and J. Kaipio, "Computational aspects of the ultra-weak variational formulation," J. Comput. Phys. **182**, 27–46 (2002).
[24]C. Farhat, I. Harari, and U. Hetmaniuk, "A discontinuous Galerkin method with plane waves and Lagrange multipliers for the solution of Helmholtz problems in the mid-frequency regime," Comput. Methods Appl. Mech. Eng. **192**, 1389–1419 (2003).
[25]G. Gabard, P. Gamallo, and T. Huttunen, "A comparison of wave-based discontinuous Galerkin, ultra-weak and least-square methods for wave problems," Int. J. Numer. Methods Eng. **85**, 380–402 (2011).
[26]E. Perrey-Debain, J. Trevelyan, and P. Bettess, "Wave boundary elements: A theoretical overview presenting applications in scattering of short waves," Eng. Anal. Boundary Elements **28**, 131–141 (2004).
[27]W. Desmet, P. Sas, and D. Vandepitte, "An indirect Trefftz method for the steady-state dynamic analysis of coupled vibro-acoustic systems," Comp. Assist. Mech. Eng. Sc. **28**, 271–288 (2001).
[28]R. Lanoye, G. Vermeir, W. Lauriks, F. Sgard, and W. Desmet, "Prediction of the sound field above a patchwork of absorbing materials," J. Acoust. Soc. Am. **123**, 793–802 (2008).
[29]H. Riou, P. Ladevéze, and L. Kovalevsky, "The variational theory of complex rays: An answer to the resolution of mid-frequency 3D engineering problems," J. Sound Vib. **332**, 1947–1960 (2013).
[30]G. Fairweather, A. Karageorghis, and P. Martin, "The method of fundamental solutions for scattering and radiation problems," Eng. Anal. Boundary Elements **27**, 759–769 (2003).
[31]A. El-Kacimi and O. Laghrouche, "Improvement of PUFEM for the numerical solution of high-frequency elastic wave scattering on unstructured triangular mesh grids," Int. J. Numer. Methods Eng. **84**, 330–350 (2010).
[32]T. Huttunen, P. Monk, F. Collino, and J. Kaipio, "The ultra-weak variational formulation for elastic wave problems," SIAM J. Sci. Comput. (USA) **25**, 1717–1742 (2004).
[33]E. Deckers, N.-E. Hörlin, D. Vandepitte, and W. Desmet, "A wave based method for the efficient solution of the 2d poroelastic Biot equations," Comput. Methods Appl. Mech. Eng. **201–204**, 245–262 (2012).
[34]E. Deckers, B. Van Genechten, D. Vandepitte, and W. Desmet, "Efficient treatment of stress singularities in poroelastic wave based models using special purpose enrichment functions," Comput. Struct. **89**, 1117–1130 (2011).
[35]B. Nennig, E. Perrey-Debain, and J.-D. Chazot, "The method of fundamental solutions for acoustic wave scattering by a single and a periodic array of poroelastic scatterers," Eng. Anal. Boundary Elem. **35**, 1019–1028 (2011).
[36]J. Chazot, B. Nennig, and E. Perrey-Debain, "Performances of the partition of unity finite element method for the analysis of two-dimensional interior sound fields with absorbing materials," J. Sound Vib. **332**, 1918–1929 (2013).
[37]M. Ouisse, M. Ichchou, S. Chedly, and M. Collet, "On the sensitivity analysis of porous material models," J. Sound Vib. **331**, 5292–5308 (2012).
[38]J.-D. Chazot, E. Zhang, and J. Antoni, "Acoustical and mechanical characterization of poroelastic materials using a Bayesian approach," J. Acoust. Soc. Am. **131**, 4584–4595 (2012).
[39]P. Debergue, R. Panneton, and N. Atalla, "Boundary conditions for the weak formulation of the mixed (u, p) poroelasticity problem," J. Acoust. Soc. Am. **106**, 2393 (1999).
[40]O. Laghrouche and M. Mohamed, "Locally enriched finite elements for the Helmholtz equation in two dimensions," Comput. Struct. **88**, 1469–1473 (2010).
[41]O. Laghrouche, P. Bettess, E. Perrey-Debain, and J. Trevelyan, "Wave interpolation finite elements for Helmholtz problems with jumps in the wave speed," Comput. Methods Appl. Mech. Eng. **194**, 367–381 (2005).
[42]T. Stroubolis, R. Hidajat, and I. Babuška, "The generalized finite element method for Helmholtz equation. Part II. Effect of choice of handbook functions, error due to absorbing boundary conditions and its assessment," Comput. Methods Appl. Mech. Eng. **197**, 364–380 (2008).
[43]T. Huttunen, P. Gamallo, and R. Astley, "Comparison of two wave element methods for the Helmholtz problem," Commun. Numer. Methods Eng. **25**, 35–52 (2009).
[44]C. Geuzaine and J.-F. Remacle, "Gmsh: A three-dimensional finite element mesh generator with built-in pre- and post-processing facilities," Int. J. Numer. Methods Eng. **79**, 1309–1331 (2009).
[45]W. Press, A. Teukolsky, W. Vetterling, and B. Flannery, *Numerical Recipes in Fortran* (Cambridge University Press, Cambridge, 1989), Chap. 4, 722 pp.
[46]J. Carcione, C. Morency, and J. Santos, "Computational poroelasticity—A review," Geophysics **75**, 229–243 (2010).